A scheme for representing aromatic secondary organic aerosols in chemical transport models: application to source attribution of organic aerosols over South Korea during the KORUS-AQ campaign.

J.F. Brewer[1,2], D.J. Jacob[1], S.H. Jathar[3], Y. He[3], A. Akherati[3,4], S. Zhai[1], D.S. Jo[5], A. Hodzic[5], B.A. Nault[6], P. Campuzano-Jost[7,8], J.L. Jimenez[7,8], R.J. Park[9], Y.J. Oak[9], and H. Liao[10]

[1]Harvard John A. Paulson School of Engineering and Applied Sciences, Harvard University, Cambridge, MA, USA

[2]University of Minnesota, St. Paul, MN, USA

[3]Department of Mechanical Engineering, Colorado State University, Ft. Collins, CO, USA

[4]Department of Atmospheric Sciences, Colorado State University, Ft. Collins, CO, USA

[5]National Center for Atmospheric Research (NCAR), Boulder, CO, USA

[6]Center for Aerosol and Cloud Chemistry, Aerodyne Research, Billerica, MA, USA

[7]Department of Chemistry, University of Colorado, Boulder, CO, USA

[8]Cooperative Institute for Research in Environmental Sciences, University of Colorado, Boulder, CO, USA

[9]School of Earth and Environmental Sciences, Seoul National University, Seoul, Republic of Korea

[10]Jiangsu Key Laboratory of Atmospheric Environment Monitoring and Pollution Control, Collaborative Innovation Center of Atmospheric Environment and Equipment Technology, School of Environmental Science and Engineering, Nanjing University of Information Science and Technology, Nanjing, China.

Corresponding author: Jared F. Brewer (brewe222@umn.edu)

Key Points

- We present an updated representation of aromatic organic aerosol formation incorporating advances in interpreting chamber experiments.
- Our model's improved scheme is better able to simulate organic aerosol observed during the KORUS-AQ field campaign.
- Surface-level korean organic aerosol is produced one third each by domestic and external anthropogenic emissions and natural emissions.

Abstract

We present a new volatility basis set (VBS) representation of aromatic secondary organic aerosol (SOA) for atmospheric chemistry models by fitting a statistical oxidation model with aerosol microphysics (SOM-TOMAS) to results from laboratory chamber experiments. The resulting SOM-VBS scheme also including previous work on SOA formation from semi- and intermediate volatile organic compounds (S/IVOCs) is implemented in the GEOS-Chem chemical transport model and applied to simulation of observations from the KORUS-AQ field campaign over Korea in May-June 2016. Our SOM-VBS scheme can simulate the KORUS-AQ OA observations from aircraft and surface sites better than the default schemes used in GEOS-Chem including for vertical profiles, variability, diurnal cycle, and partitioning between hydrocarbon-like OA (HOA) and oxidized OA (OOA). Our results confirm the important contributions of oxidized primary OA (OPOA) and aromatic SOA found in previous analyses of the KORUS-AQ data and show a large contribution from S/IVOCs. Model source attribution of OA in surface air over South Korea indicates one third from domestic anthropogenic emissions, with a large contribution from toluene and xylenes, one third from external anthropogenic emissions, and one third from natural emissions.

1. Introduction

Aerosol particles are of crucial importance for air quality and climate. Organic aerosols (OA) are a major and growing fraction of aerosol mass (Jimenez et al., 2009; Marais et al., 2017). Most of OA is secondary (SOA), produced in the atmosphere from the oxidation of volatile organic compounds (VOCs), but the mechanisms for SOA formation and removal are still poorly understood and model representations are uncertain (Hodzic et al., 2016; Lannuque et al., 2018; Pai et al., 2020).

OA observations made by research aircraft and from surface sites in Korea during the joint Korea-United States Air Quality Study (KORUS-AQ) in May-June 2016 (Crawford et al., 2021) offer some recent insight into this problem. The majority of OA during KORUS-AQ was oxidized OA of anthropogenic origin, with a major contribution from aromatic and low-volatility VOCs (Jordan et al., 2020; Nault et al., 2018). An ensemble of Chemical transport models (CTMs) used to simulate the KORUS-AQ conditions were found to underestimate OA relative by ~46% relative to the aircraft observations (Choi et al., 2019; Park et al., 2021), and to have little predictive capability for surface sites (Choi et al., 2019; Kumar et al., 2021). Previous CTM

studies in regions of high anthropogenic emissions similarly found little ability to reproduce observations and a general underestimate (Hodzic et al., 2020; Schroder et al., 2018; Shah et al., 2019).

Simulation of SOA in current CTMs relies on various schemes. The simplest scheme is to co-emit SOA with the parent VOC at a fixed yield (Chin et al., 2002; S. Kim et al., 2015; Pai et al., 2020), or produce it downwind with a fixed timescale for chemical aging (Hodzic & Jimenez, 2011), assuming SOA to be non-volatile and removed only by deposition. A more process-based scheme is to have SOA gaseous precursors produced from VOC oxidation partition reversibly into the aerosol on the basis of their volatility (Odum et al., 1996), and this is widely implemented in CTMs using the volatility basis set (VBS) parameterization (Ahmadov et al., 2012; Carlton et al., 2010; Dentener et al., 2006; Donahue et al., 2006; Pye et al., 2010; Shrivastava et al., 2011). Yet another scheme is to explicitly describe SOA formation as coupled to the gas-phase kinetic mechanism, though this has been done only for aqueous-phase SOA formation from biogenic isoprene (Fisher et al., 2016; Marais et al., 2016; McNeill et al., 2012) due to the lack of needed data and the large number of different VOCs responsible for anthropogenic SOA formation.

VBS and related SOA formation schemes based on gas-aerosol partitioning of semi-volatile products of VOC oxidation have relied on fitting to chamber observations of time-dependent SOA yields as a function of VOC reacted (Henze et al., 2008; Ng et al., 2007; Pye et al., 2010). Early work did not account properly for losses of SOA and precursors to chamber walls (Zhang et al., 2014), for sustained SOA formation on timescales longer than the chamber experiments (Cappa & Wilson, 2012; Jathar et al., 2015), or for the importance of Highly Oxidized Organic Molecules (HOMs) and oligomer condensation (Bianchi et al., 2019; He et al.,

2021). Cappa & Wilson (2012) developed the statistical oxidation model (SOM) to account for changing SOA yields and evolving SOA composition over time as a result of complex multi-step chemistry (Jo et al., 2013) and including wall loss effects in chamber data (Matsunaga & Ziemann, 2010). Hodzic et al. (2016) designed such a SOM scheme for application to CTMs, and further improved the representation of anthropogenic SOA by allowing for explicit formation from semi-volatile (SVOC) and intermediate-volatility (IVOC) organic compounds missing from earlier VBS schemes (Ahmadov et al., 2012; Pye et al., 2010). However, when implemented into the GEOS-Chem CTM (Hodzic et al., 2016) or the CAM-Chem CTM (Tilmes et al., 2019), the scheme still underestimates OA concentrations during KORUS-AQ (Park et al., 2021). More recently, SOM has been coupled with the TwO Moment Aerosol Sectional (TOMAS) microphysical model (SOM-TOMAS) to better account for experimental artifacts (e.g., size-dependent wall losses) and the SOA microphysics while fitting to chamber data (Akherati et al., 2020; He et al., 2020).

In this work, we update the Hodzic scheme's aromatic SOA formation terms within the GEOS-Chem CTM. We evaluate the scheme with KORUS-AQ observations and show modest improvement compared to previous VBS schemes implemented in GEOS-Chem (Pye et al., 2010; Pai et al., 2019), both in terms of fitting the variability of observations and enabling a more process-based representation. From there we examine the role of aromatic VOCs in driving SOA formation over East Asia and the implications for transport of aerosol pollution from China to Korea.

2. SOA simulation in GEOS-Chem

In this work we compare OA simulations in GEOS-Chem using different OA schemes: the Simple and Complex schemes that represent the standard options in the model, the Hodzic et al. (2016) scheme, and our updated version of the Hodzic scheme, here referred to as SOM-VBS.

2.1. Simple scheme.

In the Simple scheme, primary organic aerosol (POA) is handled with two species representing emitted and oxidized POA (EPOA and OPOA, respectively). Both species are directly emitted and EPOA converts to OPOA with a lifetime of 1.15 days (Henze et al., 2008; Pye & Seinfeld, 2010). SOA is non-volatile and is formed by atmospheric oxidation of tagged precursors with lifetimes of one day. These tagged precursors represent different source types and are emitted in proportion to proxy species: CO emissions from wildfires, biofuel, and fossil fuel combustion (Cubison et al., 2011; Hayes et al., 2015; S. Kim et al., 2015) and biogenic emissions of isoprene (S. Kim et al., 2015) and terpenes (Chin et al., 2002). In the case of anthropogenic SOA specifically, the simple scheme links SOA to CO emissions without reference to local conditions, instead of to relevant local conditions such as the presence of precursor VOCs, abundance of NO_x, and the pre-existing seed aerosol loading.

2.2 Complex scheme

The Complex scheme combines a VBS algorithm (Pye et al., 2010) with explicit aqueous-phase mechanisms for isoprene SOA (Marais et al., 2016) and nitrate-containing SOA (Fisher et al., 2016). It can be run with POA being either non-volatile (as in the simple scheme) or semi-volatile. Using the semi-volatile POA scheme allows the EPOA to reversibly partition between the gas (EPOG) and aerosol phases. This gas-phase EPOG can oxidize with OH to form

low-volatility oxidized primary organic gases which can reversibly partition to the aerosol phase as a function of volatility, seed aerosol abundance, and local conditions (Pai et al., 2020; Pye et al., 2010). The formation of SOA from oxidation of aromatics and terpenes by OH and ozone follows a standard VBS framework (Donahue et al., 2006), and this is also included for isoprene as an option. The inclusion of isoprene in both aqueous and volatility-based schemes gives the possibility for double-counting of isoprene SOA; this is discussed in detail in each of the relevant schemes but is ultimately not important in relatively isoprene-poor Korea. Different VBS yields are used in the high-NO_x and low-NO_x regimes because the VOC oxidation pathways are different, and the branching ratio between high- and low-NO_x oxidation pathways for all SOA precursors is a function of the relative abundances of HO_2 and NO and the rate coefficients of the relevant reactions (Pye & Seinfeld, 2010). Partitioning between the gas and particle phase occurs according to absorptive partitioning theory (Chung & Seinfeld, 2002; Pankow, 1994).

Aerosol precursor yields for the light aromatics (benzene, toluene, and xylene) under high-NO_x conditions are based on three-product fits (298 K effective saturation concentration C* = 1, 10, and 100 μg m^{-3}) to chamber experiment data by Ng et al. (2007). Under low-NO_x conditions, SOA production from these species is treated as a high (≥30%) constant yield of non-volatile products (Henze et al., 2008).

Naphthalene-like IVOC parameterizations for oxidized POA (OPOA) formation are from Pye and Seinfeld (2010), based on naphthalene chamber experiments by Chan et al. (2009), and are similarly represented in the high-NO_x case with a three-product fit and in the low NO_x case by a constant yield of 73% (Henze et al., 2008; Pye et al., 2010); this parameterization is only used in the semi-volatile POA configuration. This scheme is outdated, as more recent research

has shown that mobile-source IVOCs, at least, are primarily alkane-like and show significantly different NO_x dependences than a polycyclic aromatic like naphthalene (Lu et al., 2020).

The Complex scheme in GEOS-Chem also includes irreversible aqueous aerosol formation from isoprene oxidation coupled to the gas-phase kinetic mechanism (Marais et al., 2016). This can add to the isoprene VBS or supplant it; the default option is to supplant it. The dominant pathways for isoprene SOA formation are through the isoprene epoxide and glyoxal, the latter which can also be produced from the oxidation of aromatics (Bates et al., 2021).

Finally, the Complex scheme includes a mechanism for aqueous-phase formation of organo-nitrate aerosol from gas-phase organic nitrate precursors (Fisher et al., 2016). This mechanism is intended to produce monoterpene nitrates but GEOS-Chem uses the same lumped gas-phase organic nitrate precursor for monoterpenes and $>C_3$ alkanes, resulting in spurious SOA formation from alkanes. Here we split the lumped organic nitrate precursor for monoterpenes and $>C_3$ alkanes and remove the alkane branch from this SOA formation pathway. This decreases organo-nitrate aerosol formation globally by 14% and over the KORUS-AQ domain by 20%.

The complex scheme has several advantages over the simple scheme. It links the best available chamber experiments on SOA formation to the model; it makes for easy precursor apportionment; and it enables predictions of changes in SOA as emissions or meteorological conditions change. However, it is less successful at reproducing atmospheric OA observations than the Simple mechanism – while the Complex scheme can more effectively capture the variability of OA concentrations than the Simple scheme, it systematically underestimates actual OA abundances relative to both the Simple scheme and observations (Pai et al., 2020).

More recent work has shown that the interpretations of chamber experiments used in creation of the Complex scheme underestimated effects of wall loss of the gas-phase low-

180 volatility vapors (Zhang et al., 2014). Other work has illustrated the importance of
181 multigenerational oxidation in SOA formation (Cappa & Wilson, 2012; Hodzic et al., 2016;
182 Jathar et al., 2015), as well as the importance of Highly Oxidized Organic Molecules (HOMs)
183 and oligomers, all of which can impact aerosol yields as well as volatility of SOA formed from
184 different VOCs (Bianchi et al., 2019; He et al., 2021). Below, we detail a first attempt to
185 incorporate some of these principles into GEOS-Chem (Hodzic et al., 2016) followed by our
186 improvements (SOM-TOMAS scheme) based upon more recent work.
187
188 2.3 The Hodzic et al. (2016) scheme
189 Hodzic et al. (2016) updated the VBS of the Complex scheme in GEOS-Chem but this
190 was never included in the standard version of the model. Their VBS used the SOM box model
191 for all SOA precursors (Cappa et al., 2013; Cappa & Wilson, 2012; Jathar et al., 2015), except
192 for the low-volatility VOC families described below. SOM accounts for multi-generational
193 chemistry, including fragmentation and functionalization, and is much better at representing the
194 evolution of SOA yields and O:C ratios over time found in chamber experiments as well as in
195 simulating the dependence of SOA yields on carbon and oxygen numbers of the precursors
196 (Cappa et al., 2013; Cappa & Wilson, 2012). Hodzic et al. (2016) developed SOM box-model
197 parameterizations for individual chamber experiments and NO_x conditions. They then ran them
198 forward under pseudo-atmospheric conditions, fitting the VBS for each parent VOC. They used
199 six volatility bins rather than three to four in Pye et al. (2010). Unlike in Pye et al. (2010), they
200 included a dependence on pre-existing OA, for both high- and low-NO_x regimes, though this
201 dependence was only simulated at a single OA mass concentration value (10 $\mu g\ m^{-3}$). They

preserved the isoprene VBS as well as the aqueous isoprene SOA formation mechanism, on the principle that both may additively occur.

Hodzic et al. (2016) also accounted for SOA formation from emitted intermediate-volatility organic compounds (IVOCs, C* = $1x10^4$-$1x10^6$ μg m^{-3}) and semivolatile organic compounds (SVOCs, C* = 1-1000 μg m^{-3}), which have much lower volatility than typical VOCs (C* ~ 10^7 μg m^{-3}). SVOCs and IVOCs are typically not included in emissions inventories and their composition remains uncertain. The Complex scheme does not explicitly represent SVOCs but instead considers them to be part of POA, and it represents IVOC emissions only as a part of the semi-volatile POA scheme when that option is used (Pye et al., 2010).

Hodzic et al. (2016) set emissions of SVOCs and IVOCs at 60% and 20% of anthropogenic POA and NMVOC emissions, respectively, based on US data (Jathar et al. 2014), and assumed a structure of straight-chain C_{12}-C_{30} n-alkanes (Lee-Taylor et al., 2011). They then used box model simulations with the GECKO-A explicit chemical mechanism at low- and high-NOx regimes to represent SOA formation from these S/IVOCs, which were then fit to a VBS. More recent work suggests that other S/IVOCs may also contribute to aerosol formation including siloxanes and oxygenated IVOCs (McDonald et al., 2018).

It is important to note that by using a non-volatile POA scheme and including S/IVOC production of SOA, this scheme is almost certainly double counting some anthropogenic emissions, and more work is necessary to refine POA emissions. It could be argued that Hodzic et al. (2016) treat the non-volatile fraction of POA as POA, and the semi-volatile fraction as SOA. This treatment is less precise regarding the distinction between ‘secondary’ and ‘primary’ OA than that included in Pye et al. (2010) but is more consistent with how OA measurements like Aerosol Mass Spectrometry (AMS) are taken. The AMS cannot in principle distinguish

between semi-volatile oxidized POA and SOA (J. Wang et al., 2021), so maintaining the strong distinction between the two in the OA scheme seems less important.

In addition to these changes to SOA formation, Hodzic et al. (2016) added three loss processes for OA. The first is the inclusion of volatility-dependent dry and wet deposition of gas-phase aerosol precursor species from the VBS (the complex scheme uses Henry's law constants which do not vary by volatility); the second is the photolysis of SOA, which is scaled to the NO_2 photolysis frequency (J_{NO2}) and loses carbon atoms at a rate of 0.04% of J_{NO2}; and the third is an assumed heterogenous reaction with ozone at the surface of particles at a rate dependent upon both the concentration of ozone and total surface area of OA per volume.

2.4 SOM-TOMAS update to Hodzic et al. (2016) scheme

Here, we follow the Hodzic et al. (2016) scheme but include an improved representation of aromatic SOA by fitting chamber data to a SOM-TOMAS box model (Akherati et al., 2020; He et al., 2020), and then fitting the box model results to a VBS. Our version of SOM-TOMAS (Akherati et al., 2020; He et al., 2020) includes the formation of HOMs and oligomers from aromatic precursors. In low-NO_x conditions and near-surface temperatures (>253 K; Stolzenburg et al., 2018), peroxy radicals arising from VOC oxidation can auto-oxidize to form HOMs, which generally have very low saturation vapor pressure ($<10^{-4}$ ug/m^{-3}) and are known to contribute to new particle formation and growth (Bianchi et al., 2019; Mehra et al., 2020; Stolzenburg et al., 2018; S. Wang et al., 2017). High-molecular-weight oligomers have also been observed in SOA formation from aromatic compounds under low-NO_x conditions (D'Ambro et al., 2018; He et al., 2020; Sato et al., 2019).

Using SOM-TOMAS, we parameterize our VBS (referred to hereafter as SOM-VBS) using the following three steps:

1. We use SOM-TOMAS to derive OA parameterizations for aromatic species based on chamber experiments detailed in Ng et al. (2007) for benzene and m-xylene, and Zhang et al. (2014) for toluene.
2. Using SOM-TOMAS and derived parameters, we perform a combination of four pseudo-atmospheric box-model simulations, accounting for atmospherically representative existing OA background (1 μg m^{-3} for remote regions and 20 μg m^{-3} for polluted or urban regions) and NO_x chemical states (high and low-NO_x). We use an atmospherically relevant precursor abundance of 1 pptv for each species, and account for oxidation by typical OH concentration (10^6 molecules cm^{-3}) over time in order to represent SOA formation over the course of seven days. This approach is similar to methods described earlier in Hodzic et al. (2016) and He et al. (2020).
3. We fit a VBS to the SOM-TOMAS model results for each species (benzene, toluene, m-xylene) and NO_x condition, using two background OA mass concentrations (1 μg m^{-3} and 20 μg m^{-3}) covering a range of less to more polluted conditions. We have considered the effects of using a different range of seed aerosol mass concentrations on our parameterizations; this question will be further explored in Bilsback et al. (*in prep*). We use an iterative nonlinear least-squares solver to optimize the yields of gas-phase SOA precursor products in the VBS to minimize the overall error in total SOA yield.

Figure 1 shows the VBS performance for each of the three representative aromatic species (benzene, toluene, m-xylene) at high- and low-NO_x and high- and low-background OA mass concentration. The corresponding VBS yield parameters for each of the 6 volatility-classed

gas-phase products are given in Table 1. In general, our yields are slightly higher than those used in prior model implementations and considerably higher than those currently used in GEOS-Chem (Hodzic et al., 2016; Pye et al., 2010; Tsimpidi et al., 2010), but share the same general pattern of higher- and lower-yields. In particular, the low SOA yields from m-xylene under high NO_x conditions shown in Figure 1 are consistent with past studies of m-xylene OA yields (Odum et al., 1996; Xu et al., 2015). Toluene here is used as a proxy for other 7-carbon aromatic species, and m-xylene is used here as a proxy for other xylene and C8-aromatic species, an approach commonly used in past analyses (Farina et al., 2010; Hodzic et al., 2016; Jo et al., 2013; Pye et al., 2010).

We do not include an SOA aging scheme in our model for three reasons. First, the structure of the GEOS-Chem SOA scheme, with a single 'aromatic SOA' product, makes the design of such an aging scheme necessarily non-species-specific, which is at odds with our goal in using SOM-TOMAS to give species-specific SOA yield treatments. Secondly, the Hodzic scheme, on which our parameterization is based, does not use aging methods (Hodzic et al., 2016, 2020). Finally, past analyses of similar aging schemes suggested that such adjustments will lead to other biases in model performance (Heald et al., 2011; Jathar et al., 2016). Because of this choice, SOM-VBS is thus likely to result in more SOA when the gas-phase aerosol precursors

have been aged for less than two days and less SOA yield when the gas mixture has been aged for more than 3 days.

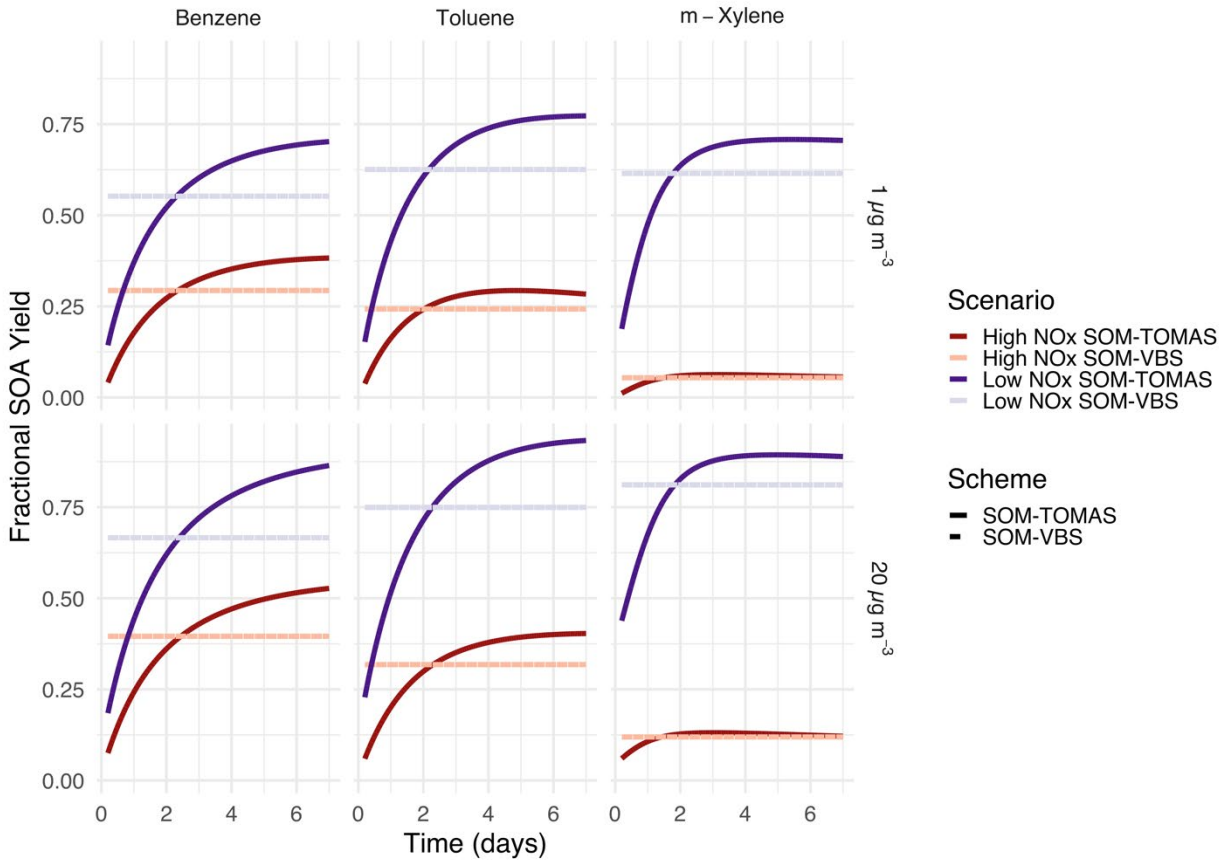

Figure 1 – Fractional mass SOA yields from the SOM-TOMAS box model scheme (solid lines) and the 6-member SOM-VBS parameterization scheme (dashed lines) for three aromatic species (benzene, m-xylene, and toluene), two NO_x conditions (high- and low-NO_x in red and blue, respectively), and two background organic aerosol concentrations (C_{OA} = 1 and 20 μg m^{-3}).

Table 1 - Yield parameters for the SOM-VBS gas-phase aromatic species at different volatilities.

Surrogate	NO_x[a]	Saturation Vapor Pressure (C*; μg m^{-3}) 0.01	0.1	1	10	100	1000
Benzene	High	0.107	0.177	0.043	0.025	0.291	0.358
Toluene[b]	High	0.130	0.109	0.021	0.026	0.193	0.521
***m*-Xylene**[c]	High	0.028	0.020	0.000	0.079	0.013	0.861
Benzene	Low	0.276	0.258	0.076	0.054	0.125	0.211
Toluene[b]	Low	0.309	0.285	0.109	0.052	0.092	0.153
***m*-Xylene**[c]	Low	0.260	0.247	0.250	0.083	0.066	0.095

[a]The branching ratio between NOx conditions (high vs low-NO_x) is determined by the fraction of organic peroxy (RO_2) radical reacting with NO (Pye et al., 2010).
[b]Toluene is used as a surrogate to represent the formation of aerosol from toluene, ethyl benzene, *i*-propyl benzene, and *n*-propyl benzene.
[c]*m*-xylene is used as a surrogate to represent the formation of aerosol from *m,p*, and *o*-xylenes, and trimethyl benzenes.

3. Simulation of KORUS-AQ observations

We use the GEOS-Chem chemical transport model version 12.0.1 (Bey et al., 2001) with the different OA schemes of Section 2 to simulate observations from the KORUS-AQ aircraft campaign and surface sites over South Korea in May-June 2016 (Choi et al., 2019). The simulation is conducted at a nested-grid resolution of 0.25° x 0.3125° over East Asia (15-55° N, 70-140° E), with dynamic boundary conditions from a global simulation at 2°x2.5° resolution. Anthropogenic emissions are from the KORUS v5 inventory in South Korea (Woo et al., 2020; http://aisl.konkuk.ac.kr/#/emission_data/korus-aq_emissions), the MEIC inventory in China (Zheng et al., 2021), and the CEDS inventory for the rest of the world (Hoesly et al., 2018). Biogenic VOC emissions are from MEGAN v2.1 (Guenther et al., 2012) and open fire emissions are from GFED 4 (Giglio et al., 2013; Randerson et al., 2012; Werf et al., 2017). POA emissions over East Asia are mainly from fossil fuel combustion, and aromatic VOCs are mainly from fuel and industrial sources. S/IVOC emissions are scaled to POA and

317 anthropogenic VOCs as previously mentioned and so are also exclusively anthropogenic, as in
318 Hodzic et al. (2016).

319 We compare the model to the KORUS-AQ observations by sampling the model output
320 along the aircraft flight tracks and at the surface site locations. We use OA observations from a
321 high-resolution time-of-flight aerosol mass spectrometer (AMS) at a one-minute resolution
322 (Nault et al., 2018) and aromatic gas concentrations from a whole air sampler (WAS)
323 (Crawford et al., 2021). A positive matrix factorization (PMF) analysis of the AMS data allows
324 us to further separate a hydrocarbon-like organic aerosol (HOA) which we equate to emitted
325 POA in GEOS-Chem, and two oxidized organic aerosols(less-oxidized and more-oxidized;
326 LO-OOA and MO-OOA) which together correspond to the total oxidized organic aerosol from
327 GEOS-Chem (i.e., the sum of SOA and oxidized POA) (Nault et al., 2018). Hourly surface
328 observations of particulate organic carbon were taken by a semi-continuous organic
329 carbon/elemental carbon analyzer (SOCEC) (Choi et al., 2019; Crawford et al., 2021).

330 As shown in Figure 2, comparison of co-located AMS and SOCEC observations at the
331 Olympic Park site show good agreement and show a mass ratio of organic matter (OM) to
332 organic carbon (OC) of roughly 2.0, with some diurnal variation. This diurnal variation shows
333 that the OM:OC ratio increases during daylight hours and decreases overnight. This increase is
334 consistent with sunlight-dependent production of higher SOA with its higher OM:OC ratio and
335 an increased importance of POA overnight. With the exception of the overnight 1.8 OM:OC
336 ratio, these OM:OC ratios are within the 1.9-2.4 range observed in other regions (Choi et al.,
337 2019; Philip et al., 2014; Turpin & Lim, 2001).

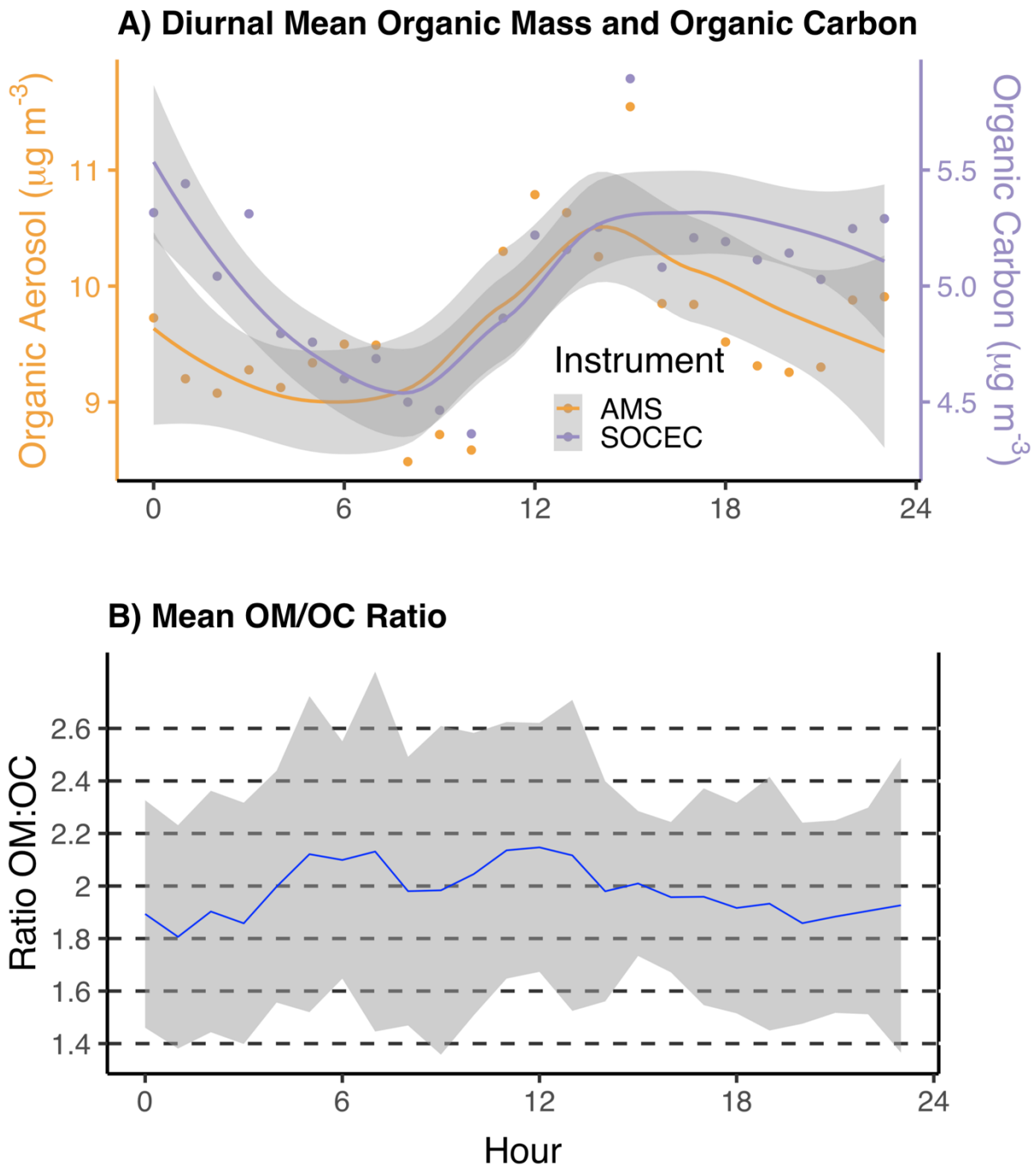

338

339 Figure 2 - Panel A) presents the mean diurnal cycle of organic aerosol and organic carbon from
340 the co-located observations of the AMS and SOCEC instruments at the Olympic Park site
341 (37.52° N, 127.12° E). Organic aerosol is shown in orange on the left axis and Organic Carbon is
342 shown in purple on the right axis; lines correspond to a loess regression of the observations with
343 uncertainty in gery. Panel B) presents the mean OM/OC ratio derived from dividing the AMS
344 observations by the SOCEC observations to get an estimate of the OM/OC ratio. As in panel B,
345 grey shading corresponds to plus or minus one standard deviation.

346 Figure 3 shows the mean vertical profiles of modeled and observed aromatic species from
347 the KORUS-AQ aircraft dataset, grouped in half-kilometer vertical bins. Figure 3 and following
348 figures detailing KORUS observations exclude data taken over the ocean. The observations here
349 are from the WAS measurements. To correspond with model definitions, observations of
350 'toluenes' include summed toluene, ethylbenzene, and both *i*- and *n*- propylbenzene mixing
351 ratios; observations of 'xylenes' correspond to the sum of *o*-, *m*-, and *p*-xylenes as well as the
352 trimethylbenzenes. On median, the model slightly underestimates benzene mixing ratios and
353 significantly underestimates both toluenes and xylenes. Overall, the simulation of these primary
354 aromatic species provides a reasonable basis for evaluating the simulation of aromatic SOA, but
355 the too-low emissions of higher aromatics in GEOS-Chem may lead to a bias in any aromatic
356 SOA contribution.

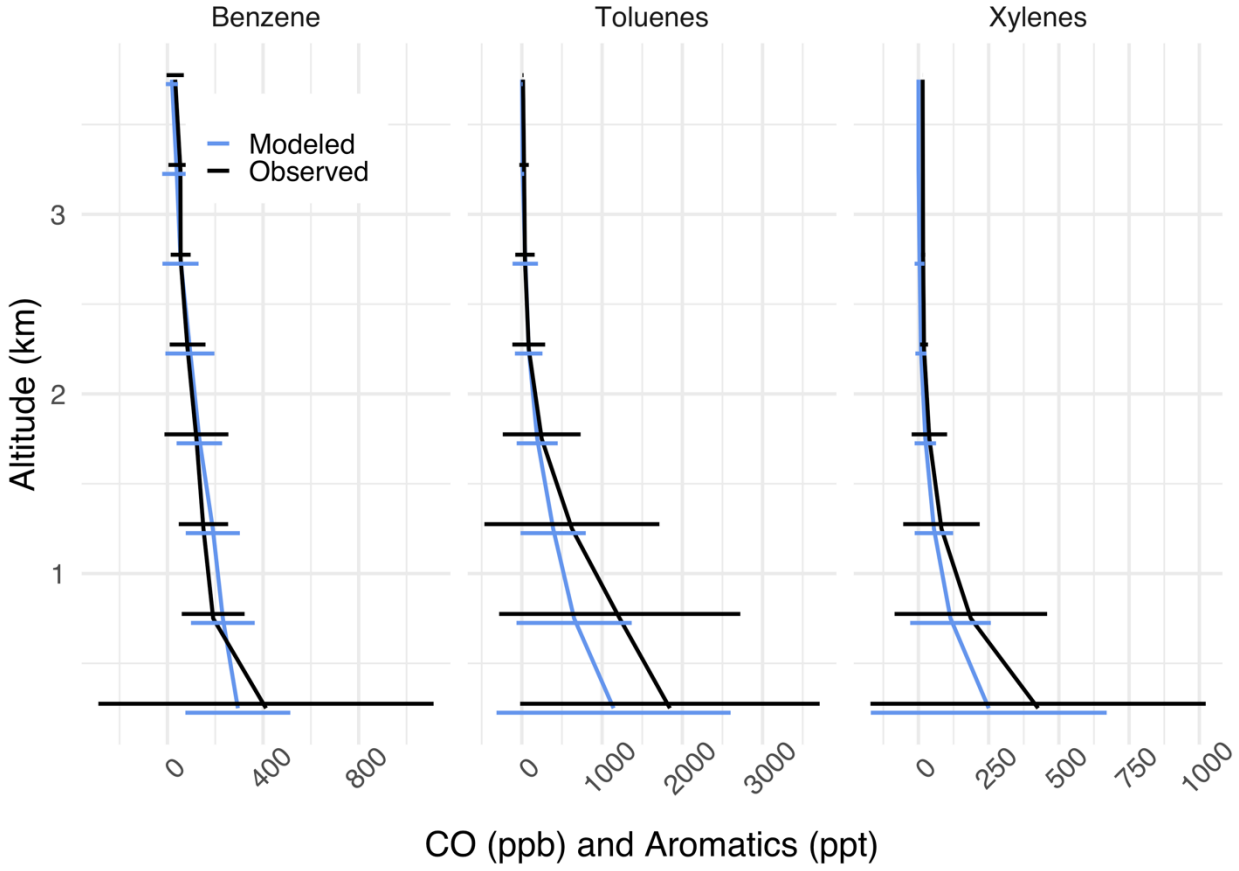

Figure 3 - Mean vertical profiles of aromatic VOC over Korea during the KORUS-AQ aircraft campaign (May-June 2016). Observations (in black) are compared to the GEOS-Chem model simulation (in blue) along the flight tracks. Horizontal bars are plus and minus one standard deviation. Note the difference in scales between panels.

Figure 4A compares mean vertical profiles of observed and modeled OA concentrations over Korea grouped in half-kilometer vertical bins. Concentrations exceed 10 µg standard m^{-3} near the surface and drop to less than 1 µg m^{-3} above 3 km. The GEOS-Chem simulations with the SOM-VBS and Hodzic schemes reproduce the observations while the other schemes are too low as previously found by Park et al. (2021). The SOM-VBS and Hodzic schemes differ only in the treatment of aromatic SOA.

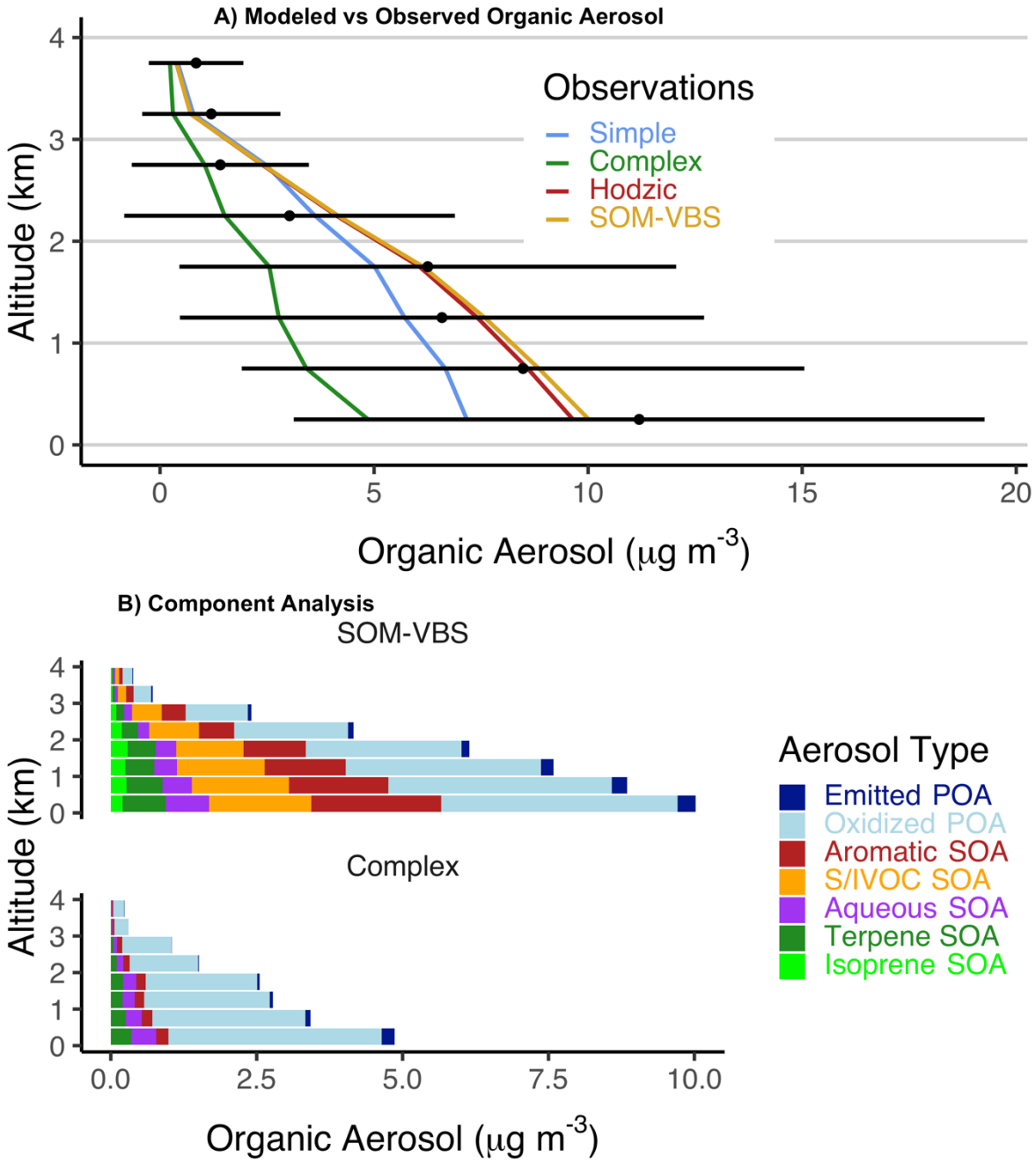

Figure 4 – Vertical distribution of organic aerosol (OA) and its GEOS-Chem model components over Korea during KORUS-AQ. Panel A) shows mean vertical profiles of organic aerosol (OA) observed by the aircraft and simulated by GEOS-Chem with the four alternative OA schemes of Section 2. Horizontal bars for the observations are one standard deviation. Panel B) shows median abundances of the different OA components simulated by GEOS-Chem for the Complex and SOM-VBS schemes.

Figure 4B shows the contributions of different OA components to the GEOS-Chem simulations using the SOM-VBS and Complex schemes. POA (mainly oxidized) is similar in both schemes and originates mainly from fuel combustion. The Simple scheme does not allow for a comparable decomposition. We see that the OA from the SOM-VBS has major contributions from aromatics and S/IVOCs. The lower concentrations in the Complex scheme are because of a much lower contribution from aromatic SOA and non-accounting of S/IVOCs SOA. Prior analysis of the KORUS data supports a large SOA contribution from aromatic and S/IVOC precursors (Nault et al., 2018).

In their multi-model analysis of the KORUS-AQ data, Park et al (2021) conclude that "models in general overestimate POA and underestimate SOA throughout the whole campaign". This conclusion depends on the definitions of POA and SOA in the modeling output. Park et al. (2021) map model POA to the AMS HOA factor and model SOA to the OOA factors, but oxidized POA in the model (OPOA) would in fact be measured as OOA (J. Wang et al., 2021). Figure 5 compares median observed vertical profiles of HOA and OOA concentrations over Korea during KORUS-AQ to the model profiles for different mapping of model components as discussed above. Total OA in the observations is dominated by OOA. We find that model SOA underestimates OOA, as reported by Park et al. (2021) but adding model OPOA produces better agreement. Model POA overestimates HOA by a factor of 4, as reported by Park et al. (2021), but removing model OPOA flips the result to a factor of 2 underestimate. That underestimate could reflect uncertainty in the aging time of EPOA and could also be accounted for by having a small fraction of model OPOA be measured as HOA, as would depend on the extent of oxidation.

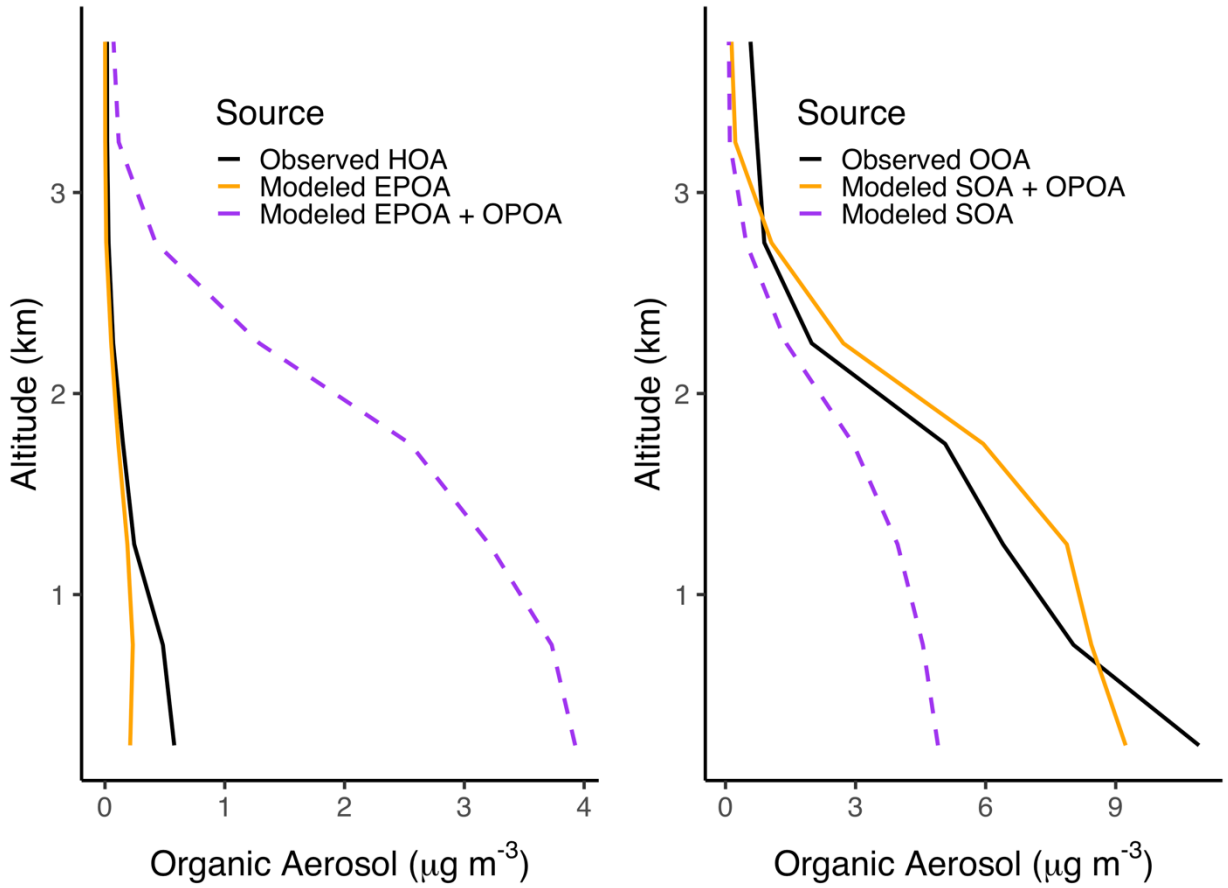

Figure 5 – Model comparison to observations of hydrocarbon-like organic aerosol (HOA) and oxidized organic aerosol (OOA) during KORUS-AQ. The Figure shows median vertical profiles of HOA and OOA concentrations over Korea measured by the Aerosol Mass Spectrometer (AMS). HOA is alternatively compared to two mappings of model OA components to these HOA vs OOA observations. In the solid orange lines, oxidized organic aerosol (OOA) is represented in GEOS-Chem as the sum of SOA + oxidized POA while hydrocarbon-like organic aerosol (HOA) corresponds to emitted POA only; in the dashed purple lines, OOA is only comprised of SOA while both emitted and oxidized POA components are compared to observed HOA. Model results are from the SOM-VBS scheme.

Figure 6 compares the median diurnal variations of simulated and observed OC aerosol at the six urban surface sites during KORUS-AQ. Aggregated, these observations show no significant diurnal variation, as in previous observations in Beijing in summer (Lin et al., 2009) that were attributed to offset between daytime production of SOA and daytime dilution from mixed layer growth. The SOM-VBS and Hodzic schemes are much better at capturing this offsetting influence because of their photochemical formation of aromatic SOA and S/IVOC

SOA, which is consistent with the pattern of OM:OC ratios observed at the Olympic Park site (Figure 2). The spurious early-morning peak in these schemes is because rising OH concentrations oxidize aromatics in a shallow mixed layer, as shown in the lower panel. The absence of such a morning maximum in the observations suggests some model error in the correlation of timing between rising photochemistry and mixed layer growth during the morning hours (Travis & Jacob, 2019).

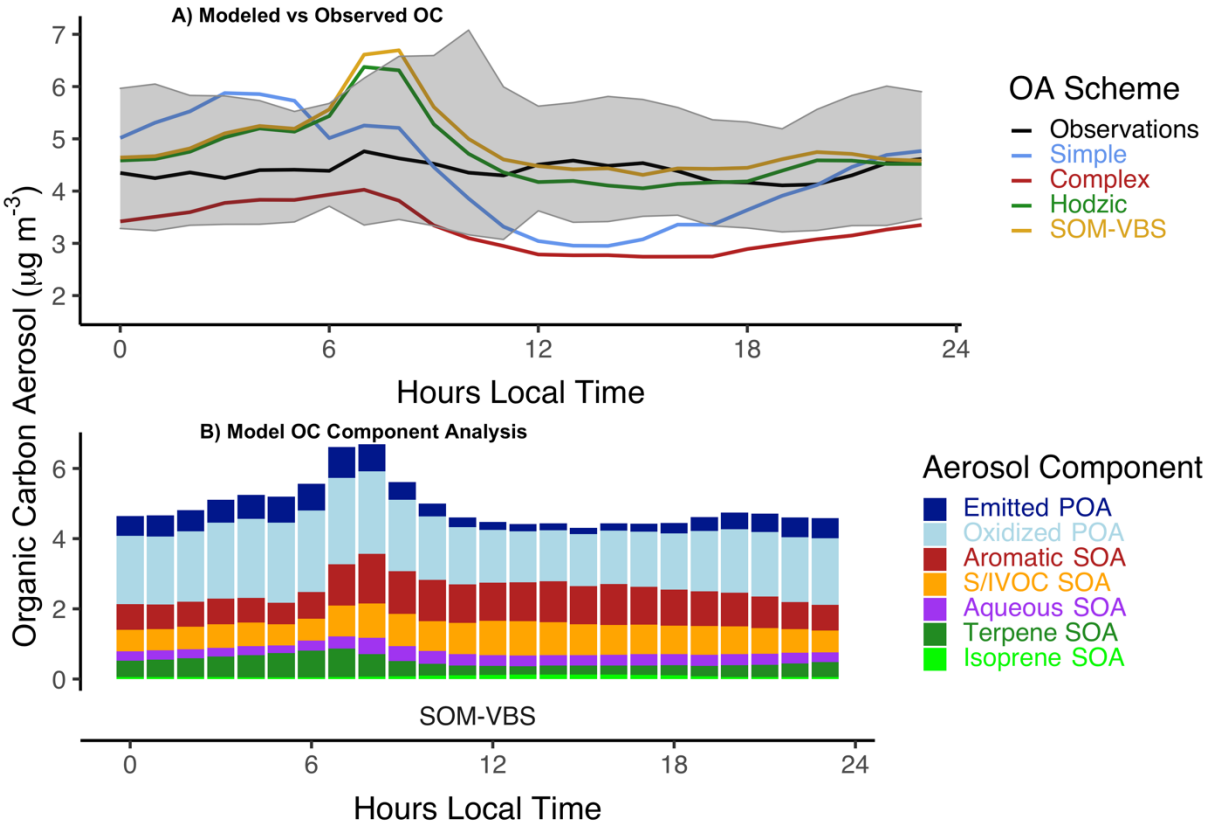

Figure 6 – Diurnal variation of organic carbon (OC) aerosol concentrations at urban sites in Korea during the KORUS-AQ campaign (8 May- 17 June 2016). The top panel shows the mean hourly concentrations for the ensemble of six urban AirKorea surface sites with OC measurements during KORUS-AQ (Choi et al., 2019): Olympic Park (37.52° N, 127.12° E), Bulkwang (37.62° N, 126.94° E), Daejeon (36.40° N, 127.40° E), Gwangju (35.23° N, 126.94° E), and Ulsan (35.58° N, 129.32° E). Observations (black, with one standard deviation spread in grey) are compared to GEOS-Chem model simulations using the four alternative organic aerosol (OA) schemes. Emitted POA is converted from organic mass (OM) to OC using a OM:OC mass ratio of 1.4, while other components have a OM:OC ratio of 2.0. The bottom panel shows the contributions of different OA components in the SOM-VBS scheme.

4. Implications for organic aerosol sources and transboundary influences

Figure 7 shows the distributions of the different OA components in surface air over the North China Plain and Korea during the KORUS-AQ period. The oxidized POA component dominates everywhere, and as pointed out above it would likely be measured by the AMS instrument as OOA. Aromatic SOA concentrations are similar in Korea and China, but concentrations of POA and S/IVOC SOA are much higher in China. In Korea, aromatics and S/IVOCs together account for 62% of total SOA during May and June. Adding in the contribution from OPOA suggests that 75% of OOA is from aromatics and S/IVOCs, consistent with the analysis of Nault et al. (2018) for Seoul. Over the North China Plain, aromatics and S/IVOCs are responsible for 53% of total SOA in May and June of 2016, and OPOA, S/IVOCs, and aromatics are 81% of total OOA (OPOA + SOA), even higher than over Korea.

Figure 7 – Mean Organic aerosol composition in surface air over East Asia during KORUS-AQ

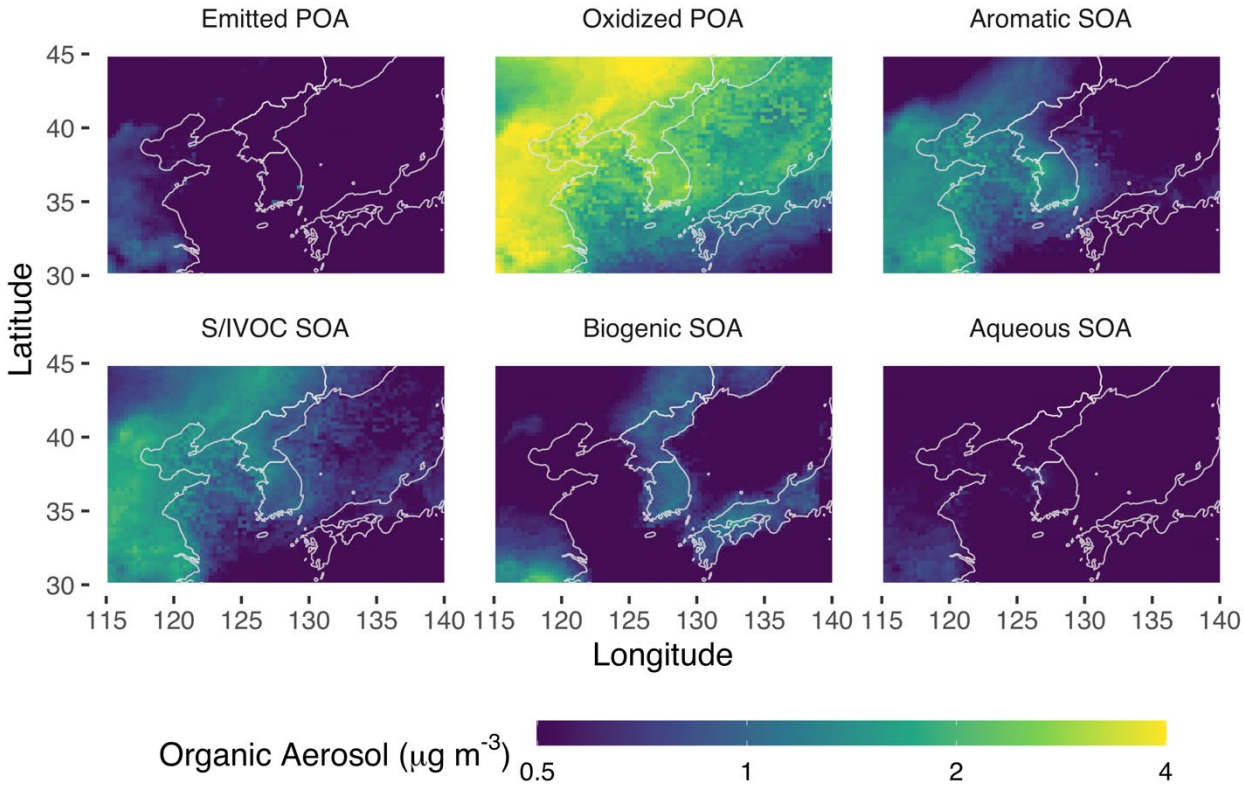

(May-June 2016) as simulated by GEOS-Chem with the SOM-VBS scheme. The 'Biogenic SOA' component includes both isoprene and terpene SOA formation from the VBS. The ''Aqueous SOA' component is mainly from isoprene but also includes some production from reactive uptake of glyoxal originating from aromatics and direct emission.

Biogenic SOA accounts for less than 13% of total OA over Korea, China, and southern Japan. This is in remarkable contrast to the US, where isoprene and terpene SOA dominate the OA aerosol load in summer (Fisher et al., 2016; P. S. Kim et al., 2015; Marais et al., 2016). Some of the conversion of emitted POA to oxidized POA could take place in the aqueous phase (J. Wang et al., 2021), but this is not included here in the aqueous SOA component.

Xylenes and toluene are the most important SOA precursor aromatics in both Eastern China and Korea. Throughout Eastern China, 43%, 42%, and 16% of Aromatic SOA are from

456 toluene, xylene, and benzene respectively; in South Korea, these figures are 45%, 47%, and 8%.
457 Benzene makes a relatively small contribution because of its long lifetime.

458 Figure 8 shows the total OA concentrations in surface air simulated by our model for
459 South Korea and the opportunities to decrease these concentrations through emission controls.
460 The middle panel shows the South Korean background, defined by zeroing anthropogenic
461 emissions of POA and VOCs in South Korea. The middle panel shows smaller peaks in South
462 Korean Background OA over the mountains of central Korea in both north and south; these are
463 from small biomass burning events included in the model. The right panel shows the natural
464 background, defined by zeroing anthropogenic emissions globally. The mean OA concentration
465 in South Korea is 8.x μg m^{-3}, and controlling domestic anthropogenic emissions could reduce it
466 by 31% to 5.5 μg m^{-3}. This South Korean background has a large contribution from external
467 anthropogenic emissions, mainly from China, and controlling these external emissions could
468 reduce OA in South Korea further down to 2.9 μg m^{-3}, mainly contributed by biogenic sources.
469 The contribution of domestic Korean emissions is largest in the Seoul and Busan coastal regions,
470 where OA concentrations are highest, and is also largest for aromatic SOA.

471 A long-standing issue has been the relative contributions of domestic and foreign
472 anthropogenic sources. Our model simulation shows that biogenic sources account for only 10%
473 of surface OA (<12% of total OA) in Korea during the KORUS-AQ period (Figure 7). We
474 further isolated the effect of domestic anthropogenic emissions by conducting a sensitivity
475 simulation removing all domestic anthropogenic emissions of aromatics, S/IVOCs, POA, glyoxal
476 and methyl glyoxal over Korea and compute the difference in modeled OA mass in the surface
477 layer. As Figure 8 shows, the influence of domestic Korean emissions on OA is most notable in
478 the Seoul and Busan coastal regions. We find that an average of 2.5 μg m^{-3} OA in the surface

layer is from domestic Korean anthropogenic emissions and a further 2.9 μg m^{-3} is from biogenic emissions, implying that the remaining 2.6 μg m^{-3} OA in the Korean boundary layer is from non-Korean anthropogenic sources. This finding is spatially variable: in the most emissions-rich areas (Seoul and the southeastern coast), which also have the highest total OA, up to 50% of surface-level OA is from domestic anthropogenic emissions sources. However, this is a considerable underestimate compared to the findings of Nault et al. (2020), who suggest that local emissions of SOA precursors 'overwhelm' foreign influences over Seoul during the KORUS-AQ period.

Domestic Korean emissions of aromatics are the most important in determining SOA, accounting for between 60-70% of aromatic SOA in the most polluted regions and 25% of total aromatic SOA on median. Domestic primary and secondary anthropogenic sources of the dicarbonyls glyoxal and methyl glyoxal account for 20% of these species on median and >50% in the most impacted areas. This implies that in the most polluted regions, it is likely incorrect to refer to these aerosols as primarily biogenic as many analyses currently do (Marais et al., 2016; Pai et al., 2020).

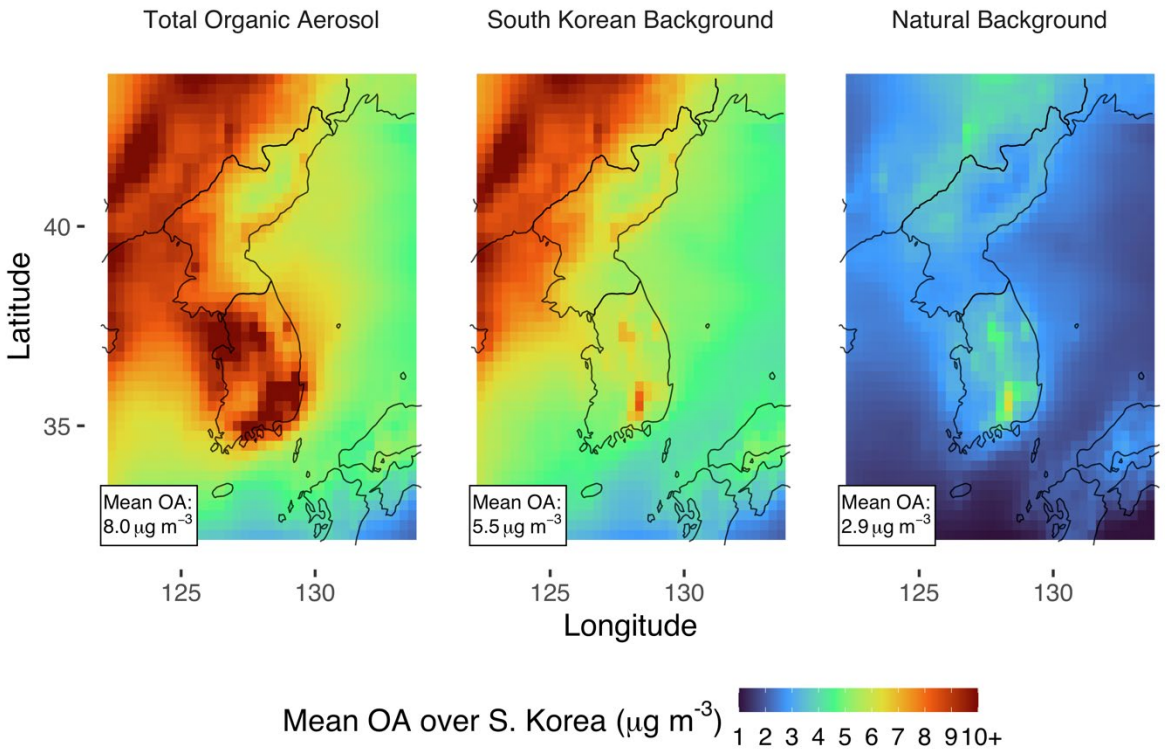

493

494 Figure 8 – Mean organic aerosol (OA) concentrations in surface air over Korea in May-June
495 2016 as simulated by GEOS-Chem with the SOM-VBS scheme. The left panel shows results
496 from our standard simulation. The middle panel shows the South Korean background
497 concentrations as determined by a simulation with domestic anthropogenic South Korean
498 emissions shut off. The right panel shows the natural background concentrations as determined
499 by a simulation with all anthropogenic emissions shut off. Mean concentrations over South
500 Korea are given inset.

501 Of the anthropogenic aerosol included in GEOS-Chem, Korean emissions of S/IVOCs
502 matter least, accounting for just 10% on median and 50% in the most impacted areas. As there
503 are no biogenic sources of S/IVOC within GEOS-Chem at this time, this implies that non-local
504 anthropogenic sources, most likely in China, are responsible for a median of 90% of the
505 S/IVOC-derived SOA observed in Korea. This points to a potential weakness of our analysis: our
506 assumptions about the emissions of S/IVOCs are based upon studies of US systems which may
507 not reflect true conditions in China or Korea (Hodzic et al., 2016; Jathar et al., 2014). Future

work will be necessary to improve the representation and speciation of S/IVOC emissions in non-US contexts, especially in China, to better understand SOA in Korea.

4. Conclusions

We present here an updated volatility basis set (SOM-VBS) for use in global chemical transport models to better represent the production of secondary organic aerosols (SOA) from the oxidation of aromatic precursors. This scheme builds on the organic aerosol (OA) scheme introduced to GEOS-Chem by Hodzic et al. (2016, 2020). We use SOM-TOMAS to re-examine previous laboratory experiments of aromatic SOA formation to correct the observed aerosol yields for gas and particle wall losses, multiple generations of oxidation, and the formation of HOMS and oligomers. These updated aerosol mass yields are then used to develop a set of VBS parameters that represent SOA formation within a global model framework.

We evaluate our scheme against aircraft and surface observations taken over Korea during the KORUS-AQ field campaign. SOM-VBS can simulate OA abundance and variability better than the default schemes used in GEOS-Chem and confirms the important contribution of aromatic SOA found in previous analyses of the KORUS-AQ data. The Simple and Complex aerosol schemes in GEOS-Chem underproduce this aromatic SOA. We also find a large SOA contribution from semi- and intermediate VOCs (S/IVOCs). The lack of diurnal cycle in OA concentrations observed at surface urban sites during KORUS-AQ supports the importance of the aromatic and S/IVOC SOA produced during daytime.

Our work corrects the previous underestimate of OA found in an intercomparison of all CTMs applied to simulation of the KORUS-AQ data (Park et al., 2021). A conclusion of that intercomparison was that the models overestimate POA and underestimate SOA, but this reflects their attribution of AMS-observed hydrocarbon-like OA (HOA) to POA and all oxidized OA

531 factors (OOA) to SOA. In fact, most of model POA is oxidized (OPOA) and would be measured
532 as OOA. By defining modeled OOA as SOA + oxidized POA, we find that GEOS-Chem is
533 unbiased in simulating observed OOA concentrations, which account for 95% of total OA.
534 Broader application of our SOM-VBS scheme to interpret sources of OA over East Asia
535 during the KORUS-AQ period finds that anthropogenic sources dominate over the whole region.
536 Oxidized POA is the most important component, followed by aromatic SOA and S/IVOC SOA.
537 Aromatic SOA is comparable in Korea and China, reflecting similar emission densities for
538 aromatic VOC precursors, but POA and S/IVOC SOA are much higher in China (S/IVOC
539 emissions are scaled to POA emissions in this implementation). Toluene and xylenes are the
540 most important aromatic precursors over both Korea and Eastern China, due to the former's
541 abundance and the latter's short lifetime.
542 We find that a third of OA in surface air in Korea is from domestic anthropogenic
543 emissions, rising to 50% in the most polluted regions (Seoul and Busan). External anthropogenic
544 emissions, mainly from China, contribute a third of surface OA in Korea, with natural emissions
545 contributing another third. Decreasing aromatic VOC emissions, principally toluene and
546 xylenes, would most effectively decrease the domestic pollution component of OA.
547

548 Acknowledgments. This work was funded by the Samsung Advanced Institute of Technology, by
549 the Harvard-NUIST Joint Laboratory for Air Quality and Climate (JLAQC), and by the NASA
550 Atmospheric Composition Campaign Data Analysis and Modeling (ACCDAM) Program

551 References:
552

553 Ahmadov, R., McKeen, S. A., Robinson, A. L., Bahreini, R., Middlebrook, A. M., Gouw, J. A.
554 de, et al. (2012). A volatility basis set model for summertime secondary organic aerosols
555 over the eastern United States in 2006. *Journal of Geophysical Research: Atmospheres*,
556 *117*(D6). https://doi.org/10.1029/2011JD016831
557 Akherati, A., He, Y., Coggon, M. M., Koss, A. R., Hodshire, A. L., Sekimoto, K., et al. (2020).
558 Oxygenated Aromatic Compounds are Important Precursors of Secondary Organic
559 Aerosol in Biomass-Burning Emissions. *Environmental Science & Technology*.
560 https://doi.org/10.1021/acs.est.0c01345
561 Bey, I., Jacob, D. J., Yantosca, R. M., Logan, J. A., Field, B. D., Fiore, A. M., et al. (2001).
562 Global Modeling of tropospheric chemistry with assimilated meteorology: Model
563 description and evaluation. *Journal of Geophysical Research*, *106*(D19), 23073–23095.
564 Bianchi, F., Kurtén, T., Riva, M., Mohr, C., Rissanen, M. P., Roldin, P., et al. (2019). Highly
565 Oxygenated Organic Molecules (HOM) from Gas-Phase Autoxidation Involving Peroxy
566 Radicals: A Key Contributor to Atmospheric Aerosol. *Chemical Reviews*, *119*(6), 3472–
567 3509. https://doi.org/10.1021/acs.chemrev.8b00395
568 Cappa, C. D., & Wilson, K. R. (2012). Multi-generation gas-phase oxidation, equilibrium
569 partitioning, and the formation and evolution of secondary organic aerosol. *Atmospheric*
570 *Chemistry and Physics*, *12*(20), 9505–9528. https://doi.org/10.5194/acp-12-9505-2012
571 Cappa, C. D., Zhang, X., Loza, C. L., Craven, J. S., Yee, L. D., & Seinfeld, J. H. (2013).
572 Application of the Statistical Oxidation Model (SOM) to Secondary Organic Aerosol
573 formation from photooxidation of C_{12} alkanes. *Atmospheric Chemistry and Physics*,
574 *13*(3), 1591–1606. https://doi.org/10.5194/acp-13-1591-2013
575 Carlton, A. G., Bhave, P. V., Napelenok, S. L., Edney, E. O., Sarwar, G., Pinder, R. W., et al.
576 (2010). Model Representation of Secondary Organic Aerosol in CMAQv4.7.
577 *Environmental Science & Technology*, *44*(22), 8553–8560.
578 https://doi.org/10.1021/es100636q
579 Chan, A. W. H., Kautzman, K. E., Chhabra, P. S., Surratt, J. D., Chan, M. N., Crounse, J. D., et
580 al. (2009). Secondary organic aerosol formation from photooxidation of naphthalene and
581 alkylnaphthalenes: implications for oxidation of intermediate volatility organic
582 compounds (IVOCs). *Atmospheric Chemistry and Physics*, *9*(9), 3049–3060.
583 https://doi.org/10.5194/acp-9-3049-2009
584 Chin, M., Ginoux, P., Kinne, S., Torres, O., Holben, B. N., Duncan, B. N., et al. (2002).
585 Tropospheric Aerosol Optical Thickness from the GOCART Model and Comparisons
586 with Satellite and Sun Photometer Measurements. *JOURNAL OF THE ATMOSPHERIC*
587 *SCIENCES*, *59*, 23.
588 Choi, J., Park, R. J., Lee, H.-M., Lee, S., Jo, D. S., Jeong, J. I., et al. (2019). Impacts of local vs.
589 trans-boundary emissions from different sectors on PM2.5 exposure in South Korea
590 during the KORUS-AQ campaign. *Atmospheric Environment*, *203*, 196–205.
591 https://doi.org/10.1016/j.atmosenv.2019.02.008
592 Chung, S. H., & Seinfeld, J. H. (2002). Global distribution and climate forcing of carbonaceous
593 aerosols. *Journal of Geophysical Research*, *107*(D19), 4407.
594 https://doi.org/10.1029/2001JD001397

595 Crawford, J. H., Ahn, J.-Y., Al-Saadi, J., Chang, L., Emmons, L. K., Kim, J., et al. (2021). The
596 Korea–United States Air Quality (KORUS-AQ) field study. *Elementa: Science of the*
597 *Anthropocene*, *9*(1), 00163. https://doi.org/10.1525/elementa.2020.00163
598 Cubison, M. J., Ortega, A. M., Hayes, P. L., Farmer, D. K., Day, D., Lechner, M. J., et al. (2011).
599 Effects of aging on organic aerosol from open biomass burning smoke in aircraft and
600 laboratory studies. *Atmospheric Chemistry and Physics*, *11*(23), 12049–12064.
601 https://doi.org/10.5194/acp-11-12049-2011
602 D'Ambro, E. L., Schobesberger, S., Zaveri, R. A., Shilling, J. E., Lee, B. H., Lopez-Hilfiker, F.
603 D., et al. (2018). Isothermal Evaporation of α-Pinene Ozonolysis SOA: Volatility, Phase
604 State, and Oligomeric Composition. *ACS Earth and Space Chemistry*, *2*(10), 1058–1067.
605 https://doi.org/10.1021/acsearthspacechem.8b00084
606 Dentener, F., Kinne, S., Bond, T., Boucher, O., Cofala, J., Generoso, S., et al. (2006). Emissions
607 of primary aerosol and precursor gases in the years 2000 and 1750 prescribed data-sets
608 for AeroCom. *Atmospheric Chemistry and Physics*, *6*(12), 4321–4344.
609 https://doi.org/10.5194/acp-6-4321-2006
610 Donahue, N. M., Robinson, A. L., Stanier, C. O., & Pandis, S. N. (2006). Coupled Partitioning,
611 Dilution, and Chemical Aging of Semivolatile Organics. *Environmental Science &*
612 *Technology*, *40*(8), 2635–2643. https://doi.org/10.1021/es052297c
613 Farina, S. C., Adams, P. J., & Pandis, S. N. (2010). Modeling global secondary organic aerosol
614 formation and processing with the volatility basis set: Implications for anthropogenic
615 secondary organic aerosol. *Journal of Geophysical Research: Atmospheres*, *115*(D9).
616 https://doi.org/10.1029/2009JD013046
617 Fisher, J. A., Jacob, D. J., Travis, K. R., Kim, P. S., Marais, E. A., Chan Miller, C., et al. (2016).
618 Organic nitrate chemistry and its implications for nitrogen budgets in an isoprene- and
619 monoterpene-rich atmosphere: constraints from aircraft
620 (SEAC⁴RS) and ground-based (SOAS) observations in the
621 Southeast US. *Atmospheric Chemistry and Physics*, *16*(9), 5969–5991.
622 https://doi.org/10.5194/acp-16-5969-2016
623 Giglio, L., Randerson, J. T., & Werf, G. R. van der. (2013). Analysis of daily, monthly, and
624 annual burned area using the fourth-generation global fire emissions database (GFED4).
625 *Journal of Geophysical Research: Biogeosciences*, *118*(1), 317–328.
626 https://doi.org/10.1002/jgrg.20042
627 Guenther, A., Jiang, X., Heald, C. L., Sakulyanontvittaya, T., Duhl, T., Emmons, L. K., & Wang,
628 X. (2012). The Model of Emissions of Gases and Aerosols from Nature version 2.1
629 (MEGAN2.1): an extended and updated framework for modeling biogenic emissions.
630 *Geoscientific Model Development*, *5*(6), 1471–1492. https://doi.org/10.5194/gmd-5-1471-
631 2012
632 Hayes, P. L., Carlton, A. G., Baker, K. R., Ahmadov, R., Washenfelder, R. A., Alvarez, S., et al.
633 (2015). Modeling the formation and aging of secondary organic aerosols in Los Angeles
634 during CalNex 2010. *Atmospheric Chemistry and Physics*, *15*(10), 5773–5801.
635 https://doi.org/10.5194/acp-15-5773-2015
636 He, Y., King, B., Pothier, M., Lewane, L., Akherati, A., Mattila, J., et al. (2020). Secondary
637 organic aerosol formation from evaporated biofuels: comparison to gasoline and
638 correction for vapor wall losses. *Environmental Science: Processes & Impacts*, *22*(7),
639 1461–1474. https://doi.org/10.1039/D0EM00103A

He, Y., Akherati, A., Nah, T., Ng, N. L., Garofalo, L. A., Farmer, D. K., et al. (2021). Particle Size Distribution Dynamics Can Help Constrain the Phase State of Secondary Organic Aerosol. *Environmental Science & Technology*, acs.est.0c05796. https://doi.org/10.1021/acs.est.0c05796

Heald, C. L., Coe, H., Jimenez, J. L., Weber, R. J., Bahreini, R., Middlebrook, A. M., et al. (2011). Exploring the vertical profile of atmospheric organic aerosol: comparing 17 aircraft field campaigns with a global model. *Atmospheric Chemistry and Physics*, *11*(24), 12673–12696. https://doi.org/10.5194/acp-11-12673-2011

Henze, D. K., Seinfeld, J. H., Ng, N. L., & Kroll, J. H. (2008). Global modeling of secondary organic aerosol formation from aromatic hydrocarbons: high- vs. low-yield pathways. *Atmos. Chem. Phys.*, 16.

Hodzic, A., & Jimenez, J. L. (2011). Modeling anthropogenically controlled secondary organic aerosols in a megacity: a simplified framework for global and climate models. *Geoscientific Model Development*, *4*(4), 901–917. https://doi.org/10.5194/gmd-4-901-2011

Hodzic, A., Kasibhatla, P. S., Jo, D. S., Cappa, C. D., Jimenez, J. L., Madronich, S., & Park, R. J. (2016). Rethinking the global secondary organic aerosol (SOA) budget: stronger production, faster removal, shorter lifetime. *Atmos. Chem. Phys.*, 25.

Hodzic, A., Campuzano-Jost, P., Bian, H., Chin, M., Colarco, P. R., Day, D. A., et al. (2020). Characterization of organic aerosol across the global remote troposphere: a comparison of ATom measurements and global chemistry models. *Atmospheric Chemistry and Physics*, *20*(8), 4607–4635. https://doi.org/10.5194/acp-20-4607-2020

Hoesly, R. M., Smith, S. J., Feng, L., Klimont, Z., Janssens-Maenhout, G., Pitkanen, T., et al. (2018). Historical (1750–2014) anthropogenic emissions of reactive gases and aerosols from the Community Emissions Data System (CEDS). *Geoscientific Model Development*, *11*(1), 369–408. https://doi.org/10.5194/gmd-11-369-2018

Jathar, S. H., Gordon, T. D., Hennigan, C. J., Pye, H. O. T., Pouliot, G., Adams, P. J., et al. (2014). Unspeciated organic emissions from combustion sources and their influence on the secondary organic aerosol budget in the United States. *Proceedings of the National Academy of Sciences*, *111*(29), 10473–10478. https://doi.org/10.1073/pnas.1323740111

Jathar, S. H., Cappa, C. D., Wexler, A. S., Seinfeld, J. H., & Kleeman, M. J. (2015). Multi-generational oxidation model to simulate secondary organic aerosol in a 3-D air quality model. *Geoscientific Model Development*, *8*(8), 2553–2567. https://doi.org/10.5194/gmd-8-2553-2015

Jathar, S. H., Cappa, C. D., Wexler, A. S., Seinfeld, J. H., & Kleeman, M. J. (2016). Simulating secondary organic aerosol in a regional air quality model using the statistical oxidation model – Part 1: Assessing the influence of constrained multi-generational ageing. *Atmospheric Chemistry and Physics*, *16*(4), 2309–2322. https://doi.org/10.5194/acp-16-2309-2016

Jimenez, J. L., Canagaratna, M. R., Donahue, N. M., Prevot, A. S. H., Zhang, Q., Kroll, J. H., et al. (2009). Evolution of Organic Aerosols in the Atmosphere. *Science*, *326*(5959), 1525–1529. https://doi.org/10.1126/science.1180353

Jo, D. S., Park, R. J., Kim, M. J., & Spracklen, D. V. (2013). Effects of chemical aging on global secondary organic aerosol using the volatility basis set approach. *Atmospheric Environment*, *81*, 230–244. https://doi.org/10.1016/j.atmosenv.2013.08.055

685 Jordan, C. E., Crawford, J. H., Beyersdorf, A. J., Eck, T. F., Halliday, H. S., Nault, B. A., et al.
686 (2020). Investigation of factors controlling PM2.5 variability across the South Korean
687 Peninsula during KORUS-AQ. *Elementa: Science of the Anthropocene*, *8*, 28.
688 https://doi.org/10.1525/elementa.424
689 Kim, P. S., Jacob, D. J., Fisher, J. A., Travis, K., Yu, K., Zhu, L., et al. (2015). Sources,
690 seasonality, and trends of southeast US aerosol: an integrated analysis of surface, aircraft,
691 and satellite observations with the GEOS-Chem chemical transport model. *Atmos. Chem.*
692 *Phys.*, *15*, 10411–10433.
693 Kim, S., Kim, S. Y., Lee, M., Shim, H., Wolfe, G. M., Guenther, A. B., et al. (2015). Impact of
694 isoprene and HONO chemistry on ozone and OVOC formation in a semirural South
695 Korean forest. *Atmospheric Chemistry and Physics*, *15*(8), 4357–4371.
696 https://doi.org/10.5194/acp-15-4357-2015
697 Kumar, N., Park, R. J., Jeong, J. I., Woo, J.-H., Kim, Y., Johnson, J., et al. (2021). Contributions
698 of international sources to PM2.5 in South Korea. *Atmospheric Environment*, *261*,
699 118542. https://doi.org/10.1016/j.atmosenv.2021.118542
700 Lannuque, V., Camredon, M., Couvidat, F., Hodzic, A., Valorso, R., Madronich, S., et al. (2018).
701 Exploration of the influence of environmental conditions on secondary organic aerosol
702 formation and organic species properties using explicit simulations: development of the
703 VBS-GECKO parameterization. *Atmospheric Chemistry and Physics*, *18*(18), 13411–
704 13428. https://doi.org/10.5194/acp-18-13411-2018
705 Lee-Taylor, J., Madronich, S., Aumont, B., Baker, A., Camredon, M., Hodzic, A., et al. (2011).
706 Explicit modeling of organic chemistry and secondary organic aerosol partitioning for
707 Mexico City and its outflow plume. *Atmospheric Chemistry and Physics*, *11*(24), 13219–
708 13241. https://doi.org/10.5194/acp-11-13219-2011
709 Lu, Q., Murphy, B. N., Qin, M., Adams, P. J., Zhao, Y., Pye, H. O. T., et al. (2020). Simulation
710 of organic aerosol formation during the CalNex study: updated mobile emissions and
711 secondary organic aerosol parameterization for intermediate-volatility organic
712 compounds. *Atmospheric Chemistry and Physics*, *20*(7), 4313–4332.
713 https://doi.org/10.5194/acp-20-4313-2020
714 Marais, E. A., Jacob, D. J., Jimenez, J. L., Campuzano-Jost, P., Day, D. A., Hu, W., et al. (2016).
715 Aqueous-phase mechanism for secondary organic aerosol formation from isoprene:
716 application to the southeast United States and co-benefit of SO_2 emission controls.
717 *Atmospheric Chemistry and Physics*, *16*(3), 1603–1618. https://doi.org/10.5194/acp-16-
718 1603-2016
719 Marais, E. A., Jacob, D. J., Turner, J. R., & Mickley, L. J. (2017). Evidence of 1991–2013
720 decrease of biogenic secondary organic aerosol in response to SO_2 emission controls.
721 *Environmental Research Letters*, *12*(5), 054018. https://doi.org/10.1088/1748-
722 9326/aa69c8
723 Matsunaga, A., & Ziemann, P. J. (2010). Gas-Wall Partitioning of Organic Compounds in a
724 Teflon Film Chamber and Potential Effects on Reaction Product and Aerosol Yield
725 Measurements. *Aerosol Science and Technology*, *44*(10), 881–892.
726 https://doi.org/10.1080/02786826.2010.501044
727 McDonald, B. C., de Gouw, J. A., Gilman, J. B., Jathar, S. H., Akherati, A., Cappa, C. D., et al.
728 (2018). Volatile chemical products emerging as largest petrochemical source of urban
729 organic emissions. *Science*, *359*(6377), 760–764. https://doi.org/10.1126/science.aaq0524

McNeill, V. F., Woo, J. L., Kim, D. D., Schwier, A. N., Wannell, N. J., Sumner, A. J., & Barakat, J. M. (2012). Aqueous-Phase Secondary Organic Aerosol and Organosulfate Formation in Atmospheric Aerosols: A Modeling Study. *Environmental Science & Technology*, *46*(15), 8075–8081. https://doi.org/10.1021/es3002986

Mehra, A., Wang, Y., Krechmer, J. E., Lambe, A., Majluf, F., Morris, M. A., et al. (2020). Evaluation of the chemical composition of gas- and particle-phase products of aromatic oxidation. *Atmospheric Chemistry and Physics*, *20*(16), 9783–9803. https://doi.org/10.5194/acp-20-9783-2020

Nault, B. A., Campuzano-Jost, P., Day, D. A., Schroder, J. C., Anderson, B., Beyersdorf, A. J., et al. (2018). Secondary organic aerosol production from local emissions dominates the organic aerosol budget over Seoul, South Korea, during KORUS-AQ. *Atmospheric Chemistry and Physics*, *18*(24), 17769–17800. https://doi.org/10.5194/acp-18-17769-2018

Ng, N. L., Kroll, J. H., Chan, A. W. H., Chhabra, P. S., Flagan, R. C., & Seinfeld, J. H. (2007). Secondary organic aerosol formation from m-xylene, toluene, and benzene. *Atmos. Chem. Phys.*, 14.

Odum, J. R., Hoffmann, T., Bowman, F., Collins, D., Flagan, R. C., & Seinfeld, J. H. (1996). Gas/Particle Partitioning and Secondary Organic Aerosol Yields. *Environ Sci Technol*, *30*, 2580–2585.

Pai, S. J., Heald, C. L., Pierce, J. R., Farina, S. C., Marais, E. A., Jimenez, J. L., et al. (2020). An evaluation of global organic aerosol schemes using airborne observations. *Atmospheric Chemistry and Physics*, *20*(5), 2637–2665. https://doi.org/10.5194/acp-20-2637-2020

Pankow, J. F. (1994). An absorption model of gas/particle partitioning of organic compounds in the atmosphere. *Atmospheric Environment*, *28*(2), 185–188. https://doi.org/10.1016/1352-2310(94)90093-0

Park, R. J., Oak, Y. J., Emmons, L. K., Kim, C.-H., Pfister, G. G., Carmichael, G. R., et al. (2021). Multi-model intercomparisons of air quality simulations for the KORUS-AQ campaign. *Elementa: Science of the Anthropocene*, *9*(1), 00139. https://doi.org/10.1525/elementa.2021.00139

Philip, S., Martin, R. V., Pierce, J. R., Jimenez, J. L., Zhang, Q., Canagaratna, M. R., et al. (2014). Spatially and seasonally resolved estimate of the ratio of organic mass to organic carbon. *Atmospheric Environment*, *87*, 34–40. https://doi.org/10.1016/j.atmosenv.2013.11.065

Pye, H. O. T., & Seinfeld, J. H. (2010). A global perspective on aerosol from low-volatility organic compounds. *Atmospheric Chemistry and Physics*, *10*(9), 4377–4401. https://doi.org/10.5194/acp-10-4377-2010

Pye, H. O. T., Chan, A. W. H., Barkley, M. P., & Seinfeld, J. H. (2010). Global modeling of organic aerosol: the importance of reactive nitrogen (NOx and NO3). *Atmospheric Chemistry and Physics*, *10*(22), 11261–11276. https://doi.org/10.5194/acp-10-11261-2010

Randerson, J. T., Chen, Y., Werf, G. R. van der, Rogers, B. M., & Morton, D. C. (2012). Global burned area and biomass burning emissions from small fires, *Journal of Geophysical Research: Biogeosciences*. Retrieved from https://agupubs.onlinelibrary.wiley.com/doi/full/10.1029/2012JG002128

Sato, K., Fujitani, Y., Inomata, S., Morino, Y., Tanabe, K., Hikida, T., et al. (2019). A study of volatility by composition, heating, and dilution measurements of secondary organic

aerosol from 1,3,5-trimethylbenzene. *Atmospheric Chemistry and Physics*, *19*(23), 14901–14915. https://doi.org/10.5194/acp-19-14901-2019

Schroder, J. C., Campuzano-Jost, P., Day, D. A., Shah, V., Larson, K., Sommers, J. M., et al. (2018). Sources and Secondary Production of Organic Aerosols in the Northeastern United States during WINTER. *Journal of Geophysical Research: Atmospheres*, *123*(14), 7771–7796. https://doi.org/10.1029/2018JD028475

Shah, V., Jaeglé, L., Jimenez, J. L., Schroder, J. C., Campuzano-Jost, P., Campos, T. L., et al. (2019). Widespread Pollution From Secondary Sources of Organic Aerosols During Winter in the Northeastern United States. *Geophysical Research Letters*, *46*(5), 2974–2983. https://doi.org/10.1029/2018GL081530

Shrivastava, M., Fast, J., Easter, R., Gustafson, W. I., Zaveri, R. A., Jimenez, J. L., et al. (2011). Modeling organic aerosols in a megacity: comparison of simple and complex representations of the volatility basis set approach. *Atmospheric Chemistry and Physics*, *11*(13), 6639–6662. https://doi.org/10.5194/acp-11-6639-2011

Stolzenburg, D., Fischer, L., Vogel, A. L., Heinritzi, M., Schervish, M., Simon, M., et al. (2018). Rapid growth of organic aerosol nanoparticles over a wide tropospheric temperature range. *Proceedings of the National Academy of Sciences*, *115*(37), 9122–9127. https://doi.org/10.1073/pnas.1807604115

Tilmes, S., Hodzic, A., Emmons, L. K., Mills, M. J., Gettelman, A., Kinnison, D. E., et al. (2019). Climate Forcing and Trends of Organic Aerosols in the Community Earth System Model (CESM2). *Journal of Advances in Modeling Earth Systems*, *11*(12), 4323–4351. https://doi.org/10.1029/2019MS001827

Travis, K. R., & Jacob, D. J. (2019). Systematic bias in evaluating chemical transport models with maximum daily 8 h average (MDA8) surface ozone for air quality applications: a case study with GEOS-Chem v9.02. *Geoscientific Model Development*, *12*(8), 3641–3648. https://doi.org/10.5194/gmd-12-3641-2019

Tsimpidi, A. P., Karydis, V. A., Zavala, M., Lei, W., Molina, L., Ulbrich, I. M., et al. (2010). Evaluation of the volatility basis-set approach for the simulation of organic aerosol formation in the Mexico City metropolitan area. *Atmos. Chem. Phys.*, 22.

Turpin, B. J., & Lim, H.-J. (2001). Species Contributions to PM2.5 Mass Concentrations: Revisiting Common Assumptions for Estimating Organic Mass. *Aerosol Science and Technology*, *35*(1), 602–610. https://doi.org/10.1080/02786820119445

Wang, J., Ye, J., Zhang, Q., Zhao, J., Wu, Y., Li, J., et al. (2021). Aqueous production of secondary organic aerosol from fossil-fuel emissions in winter Beijing haze. *Proceedings of the National Academy of Sciences*, *118*(8), e2022179118. https://doi.org/10.1073/pnas.2022179118

Wang, S., Wu, R., Berndt, T., Ehn, M., & Wang, L. (2017). Formation of Highly Oxidized Radicals and Multifunctional Products from the Atmospheric Oxidation of Alkylbenzenes. *Environmental Science & Technology*, *51*(15), 8442–8449. https://doi.org/10.1021/acs.est.7b02374

Werf, G. R. van der, Randerson, J. T., Giglio, L., Leeuwen, T. T. van, Chen, Y., Rogers, B. M., et al. (2017). Global fire emissions estimates during 1997–2016. *Earth System Science Data*, *9*(2), 697–720. https://doi.org/10.5194/essd-9-697-2017

Woo, J.-H., Kim, Y., Kim, H.-K., Choi, K.-C., Eum, J.-H., Lee, J.-B., et al. (2020). Development of the CREATE Inventory in Support of Integrated Climate and Air Quality Modeling for Asia. *Sustainability*, *12*(19), 7930. https://doi.org/10.3390/su12197930

Xu, J., Griffin, R. J., Liu, Y., Nakao, S., & Cocker, D. R. (2015). Simulated impact of NO x on SOA formation from oxidation of toluene and m -xylene. *Atmospheric Environment*, *101*, 217–225. https://doi.org/10.1016/j.atmosenv.2014.11.008

Zhang, X., Cappa, C. D., Jathar, S. H., McVay, R. C., Ensberg, J. J., Kleeman, M. J., & Seinfeld, J. H. (2014). Influence of vapor wall loss in laboratory chambers on yields of secondary organic aerosol. *Proceedings of the National Academy of Sciences*, *111*(16), 5802–5807. https://doi.org/10.1073/pnas.1404727111

Zheng, B., Cheng, J., Geng, G., Wang, X., Li, M., Shi, Q., et al. (2021). Mapping anthropogenic emissions in China at 1 km spatial resolution and its application in air quality modeling. *Science Bulletin*, *66*(6), 612–620. https://doi.org/10.1016/j.scib.2020.12.008